ACS OMEGA

http://pubs.acs.org/journal/acsodf

Article

Large-Scale Preparation of Carboxylated Cellulose Nanocrystals and Their Application for Stabilizing Pickering Emulsions

Yikang Liu, Yuan Wei,* Yingying He, Yangyang Qian,* Chunyu Wang, and Gang Chen*

Cite This: *ACS Omega* 2023, 8, 15114−15123

Read Online

ACCESS | Metrics & More | Article Recommendations | Supporting Information

ABSTRACT: Cellulose nanocrystals (CNCs) with varied unique properties have been widely used in emulsions, nanocomposites, and membranes. However, conventional CNCs for industrial use were usually prepared through acid hydrolysis or heat-controlled methods with sulfuric acid. This most commonly used acid method generally suffers from low yields, poor thermal stability, and potential environmental pollution. Herein, we developed a high-efficiency and large-scale preparation strategy to produce carboxylated cellulose nanocrystals (Car-CNCs) via carboxymethylation-enhanced ammonium persulfate (APS) oxidation. After carboxymethylation, the wood fibers could form unique "balloon-like" structures with abundant exposed hydroxy groups, which facilitated exfoliating fibril bundles into individual nanocrystals during the APS oxidation process. The production process under controlled temperature, time period, and APS concentrations was optimized and the resultant Car-CNCs exhibited a typical structure with narrow diameter distributions. In particular, the final Car-CNCs exhibited excellent thermal stability (≈346.6 °C) and reached a maximum yield of 60.6%, superior to that of sulfated cellulose nanocrystals (Sul-CNCs) prepared by conventional acid hydrolysis. More importantly, compared to the common APS oxidation, our two-step collaborative process shortened the oxidation time from more than 16 h to only 30 min. Therefore, our high-efficiency method may pave the way for the up-scaled production of carboxylated nanocrystals. More importantly, Car-CNCs show potential for stabilizing Pickering emulsions that can withstand changeable environments, including heating, storage, and centrifugation, which is better than the conventional Sul-CNC-based emulsions.

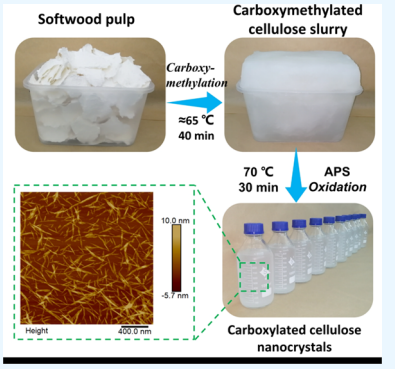

1. INTRODUCTION

Cellulose, as the most abundant natural biopolymer on the earth, is extracted from various sources including wood fibers (hard or soft wood), nonwood fibers (seed, bast, cane, leaf, straw, or fruit), bacterial, algae, and even some tunicates.[1] Within the family of cellulose nanoscale derivatives, cellulose nanocrystals (CNCs) are especially attractive owing to their unique features, such as renewability, biocompatibility, biodegradability, and ease of chemical modification.[2−6] Therefore, CNCs have been widely used in the industry and research areas, such as pickering emulsion, papermaking, food packaging, and biomedical engineering, etc.[7−12]

In order to extract CNCs, the intra- and intermolecular hydrogen bonds between the cellulose chains that consist of linear molecules β-D-glucopyranosyl units must be overcome by chemical reactions, mechanical defibrillation, enzymatic hydrolysis, ionic liquids, deep eutectic solvents, or a combination of these techniques, etc.[13−16] Among them, sulfuric acid hydrolysis is a low energy- and time-consuming method and easy to destroy the amorphous portions' hydrogen bonds of natural cellulose, producing highly stereo-regular and crystalline sulfated cellulose nanocrystals (Sul-SCNCs).[17] Moreover, the sulfuric acid hydrolysis can introduce abundant negative-charged sulfate half-ester groups on the surface of cellulose chains, which promote the CNC's suspension dispersion and avoid aggregation. However, some shortcomings also need to be noted, such as the requirement of large amounts of H_2SO_4 (9 kg H_2SO_4 per kilogram CNCs), low yields of less than 30%, potential environmental pollution, and poor thermal stability of the CNCs.[9,11,14,18−21]

Alternatively, the ammonium persulfate (APS) oxidation method was considered as a potential route to improve acid hydrolysis. APS, as a green chemical reagent with low cost, low long-term toxicity, and high solubility, is able to offer excellent thermal stability to CNCs.[9] Leung et al. first attempted the isolation of carboxylated CNCs by one-step APS oxidation from hemp, flax, and triticale.[22] During the oxidation process, once heated, the persulfate (HSO_4^-), peroxide free radicals ($SO_4^{\cdot-}$), and hydrogen peroxide (H_2O_2) were generated immediately to disintegrate CNCs and eliminate non-cellulosic components. Another advantage of this method is that the as-prepared CNCs exhibited a more homogeneous structure with

Received: December 28, 2022
Accepted: April 6, 2023
Published: April 20, 2023

© 2023 The Authors. Published by American Chemical Society

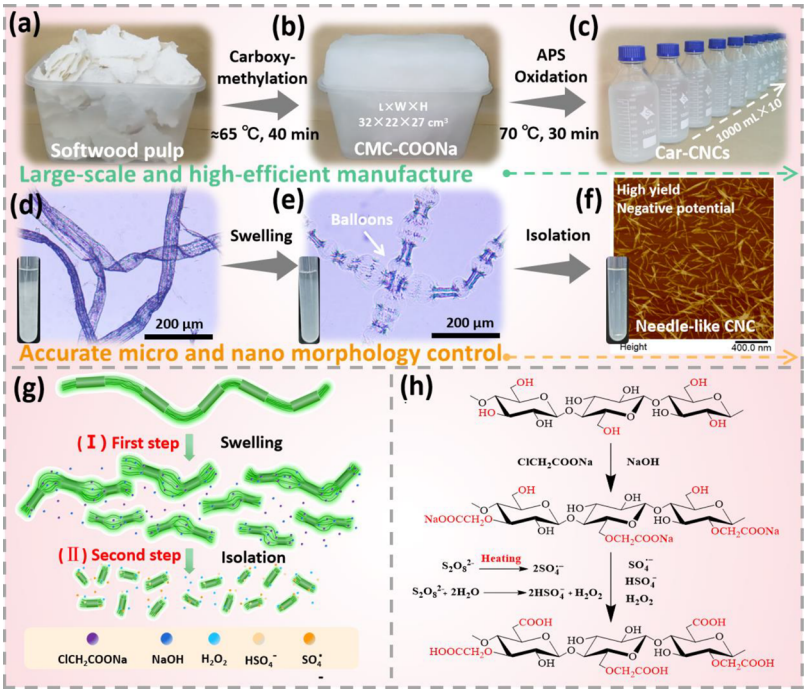

Figure 1. (a–c) Schematic illustrating the preparation of Car-CNCs through carboxymethylation and APS oxidation. (d–f) Microscopic morphologies of raw fibers (softwood pulp), carboxymethylated cellulose fibers (CMC-COONa), and Car-CNCs. (g, h) Schematic illustrating the carboxymethylation swelling pretreatment and APS oxidation mechanism on the cellulose chains.

a diameter of 5 nm and a length of 150 nm.[23] Since 2011, a number of articles about the preparation of carboxylated CNCs by one-step APS oxidation from various lignocellulosic sources, such as bleached northern softwood kraft pulp,[24] bleached birch kraft pulp,[25] kapok fibers,[26] lemon (*Citrus limon*) seeds,[27] cotton linters,[11,28] cotton pulp,[29] tunicate,[30] jute fiber,[18] sugarcane bagasse,[31] lyocell fibers,[32] have been published. However, the high time-consuming oxidation procedures (16–24 h) have reduced the production efficiency and hindered large-scale applications.[9,18,29] Therefore, it is still a challenge to develop an effective and scalable APS approach to produce high-performance CNCs.

As is known, both 2,2,6,6-tetramethylpiperidine-1-oxyl radical (TEMPO)-mediated oxidation and carboxymethylation pretreatment have been used for improving the cellulose nanofibrillation efficiency via breaking the inter/intramolecular hydrogen bonds between cellulose chains and converting the alcohol hydroxy groups to sodium carboxylate groups.[33,34] The isolation of nanocellulose by TEMPO-oxidation pretreatment is energy-saving with less energy consumption demand, but the oxidation capacity is still limited since it can only position-selectively oxidize C_6-primary alcohol groups of cellulose while the hydroxyl groups at C_2 and C_3 kept intact.[35] Moreover, TEMPO is a toxic catalyst that will cause a negative footprint on the environment. Compared to TEMPO-mediated oxidation, carboxymethylation pretreatment has relatively less pollution and higher hydroxyl conversion capacity. During carboxymethylation, the C_6, C_2, and C_3 positions on the cellulose fiber carried out nonselective reactions, thus leading to a high carboxyl content, reducing adhesion between the fibrils, and facilitating the microfibril separation.[36−38] So far, to the best of our knowledge, no study has investigated the isolation of CNCs by combining carboxymethylation pretreatment and the APS oxidation method.

In this study, the goal was to make up for the disadvantage of one-step APS oxidation and further improve the preparation efficiency of CNCs. First, we introduced a scalable carboxymethylation pretreatment step, which could facilitate the swelling of wood cell walls and expose more C_6 hydroxy groups. Then, APS oxidation was used to exfoliate fibril bundles into individual nanocrystals. The effects of APS oxidation conditions, such as time, temperature, and concentration on the yield were systematically studied to optimize the preparation process and product quality. A series of characterizations were conducted to investigate surface morphology, crystal structures, and thermal stability. Besides, compared to the conventional Sul-CNCs, our resultant carboxylated cellulose nanocrystals (Car-CNCs) exhibited high preparation efficiency and excellent performance, demonstrating great potential for scalable production. Another appealing feature of our Car-CNCs is the higher zeta potential than conventional Sul-CNCs, which can stabilize the Pickering emulsions without adding additional metal salts to adjust the electrostatic repulsion effect. The emulsions stabilized by Car-CNCs can withstand changeable environments, including heating, storage, and centrifugation, superior to the Sul-CNC-based emulsions. Thus, the Car-CNCs were explored as promising candidates for Sul-CNCs for preparing stable Pickering emulsions.

2. EXPERIMENTAL SECTION

2.1. Materials. Bleached softwood kraft pulp with a zeta potential value of −15.6 mV was purchased by Metsä Fiber China, and the α-cellulose content was ∼95%. APS (A.R.) and sodium hydroxide (NaOH, A.R.) were purchased from the Tianjin damao chemical reagent factory (Tianjing, China). Sulfuric acid (95% ∼ 98%) was purchased from Guangdong Guangxian Reagent Technology Co., Ltd. (Zhaoqing, China). Sodium chloroacetate (MCA, A.R.) was obtained from

https://doi.org/10.1021/acsomega.2c08239
ACS Omega 2023, 8, 15114−15123

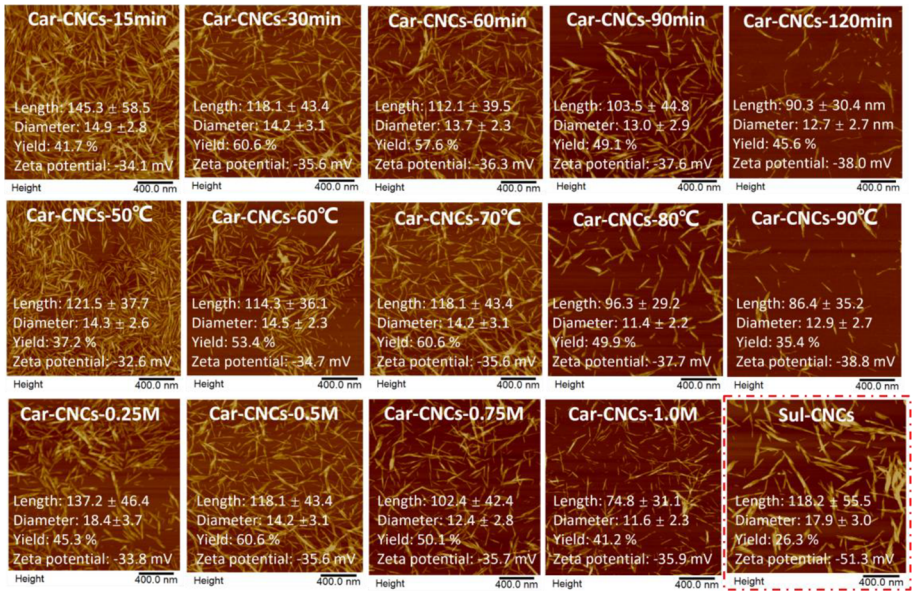

Figure 2. AFM images of the Car-CNCs under different oxidation times, APS concentrations, and reaction temperatures, as well as the AFM image of Sul-CNCs prepared at 45 °C for 70 min.

Shanghai Maclin Biochemical Technology Co., Ltd. (Shanghai, China). Liquid Paraffin (LP) was supplied from Jiangsu Qiangsheng Functional Chemical Co., Ltd. (Jiangsu, China). All reagents were used as received without further purification.

2.2. Preparation of Cellulose Nanocrystals. *2.2.1. Preparation of Carboxymethylated Cellulose Fibers.* Carboxymethylated cellulose (CMC) fibers with sodium carboxylate groups (CMC-COONa) were fabricated according to our previously described methods.[39] Briefly, 25 g of bleached softwood pulp (raw fibers) was mixed with 384 mL of ethanol in a high concentration-stirred reactor for 20 min and then NaOH solution (12.5 g) dissolved in 317 g of ethanol was added into the mixture. After that, the mixture was heated to 65 °C and followed by adding 30 g of MCA solution (w_{MCA}/w_{water} = 1:1). Subsequently, the above dispersion with ≈4 wt % of pulp consistency was stirred for 40 min at 65 °C. Finally, the CMC-COONa slurry was obtained by washing it with water in a 600-mesh filter. The carboxylate content and zeta potential value of the CMC-COONa slurry were 1.5 mmol/g and −37.6 mV, respectively. Besides, the carboxymethylation process in this study can be scalable and has been applied in the factory, as shown in Figure S1.

2.2.2. Preparation of Car-CNCs. Car-CNCs were extracted from the CMC-COONa slurry with APS. In brief, 10 g of dried CMC-COONa slurry was added to 500 mL of APS aqueous solution (0.25, 0.5, 0.75, and 1.0 mol L^{-1}) and reacted at the setting temperature (T = 50−90 °C) for different oxidation periods (15, 30, 60, 90, and 120 min). Subsequently, the suspension was centrifuged for 10 min at 10,000 rpm for several cycles until the supernatant turned turbid. Then, the obtained cellulose nanocrystal suspension was poured into dialysis membrane tubes (molecular weight cut off 10,000) and dialyzed for 1 week. Finally, the suspension was collected and denoted Car-CNCs-X, where X represents the different oxidation parameters, such as concentrations of APS, reaction temperatures, and oxidation periods. The detailed information is shown in Table S1.

2.2.3. Fabrication of Sul-CNCs by Acid Hydrolysis. For comparison, the nanocrystal suspension with sulfate half ester groups (Sul-CNCs) was prepared as previously reported methods.[40,41] Bleached softwood pulp was added to the 64% w/w sulfuric acid (the ratio of w_{fibers}/V_{acid} = 1:10 g/mL) under vigorous agitation and reacted at 45 °C for 70 min. Then, the mixture was diluted and centrifuged. For further purification, the obtained Sul-CNC suspension was also dialyzed for 1 week. After dialysis, the Sul-CNC suspension was collected and stored at 4 °C for further use.

3. RESULTS AND DISCUSSION

3.1. Preparation Strategy and Mechanism of the Car-CNCs. In our study, we combined a carboxymethylation pretreatment and the APS oxidation process to improve the preparation efficiency of CNCs. As shown in Figures 1a,b and S1, our first step was to introduce a scalable carboxymethylation swelling pretreatment, which can expose more hydroxy groups and provide more oxidation sites for further APS oxidation process.

We measured the optical microscopy images and corresponding size distributions of softwood pulp and carboxymethylated cellulose fibers (CMC-COONa), respectively. Figures 1d and S2a,b show that the raw fibers exhibit a spindly hollow structure with an average length of 2501 μm and a width of 29.4 μm. After carboxymethylation treatment, the CMC-COONa exhibited balloon-like and exfoliated structures (Figures 1e and S3). Meanwhile, the length of CMC-COONa reduced to 1415 μm, while the width expanded to 45.1 μm (Figure S2c,d). Most disintegrated fibrils (stretched out from the S1 and S2 layers) are contained inside the balloons and tend to form parallel stripes across the balloons. This change of alternating microfibril arrangements caused by full swelling behavior could facilitate the subsequent extraction of CNCs effectively. Then, APS oxidation was used to exfoliate fibril bundles into individual nanocrystals (Figure 1f).

The formation mechanism and dimensional change of the balloon structures could be explained in Figure 1g. As the carboxylic anion accumulated on the fiber surface, the electrostatic repulsive force become stronger and led to the ballooning or breakage of the fiber cell walls. As a result, the

https://doi.org/10.1021/acsomega.2c08239
ACS Omega 2023, 8, 15114−15123

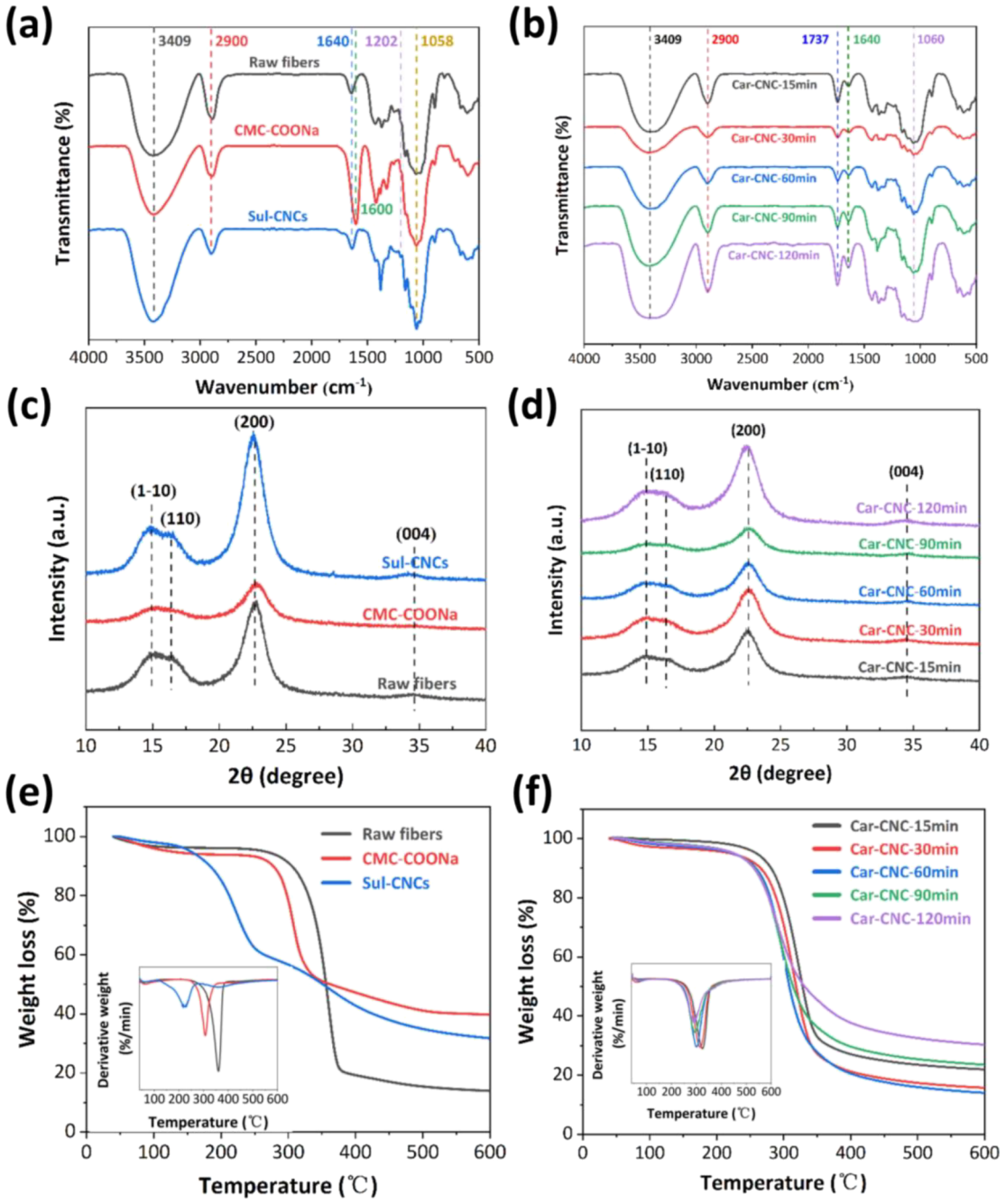

Figure 3. FT-IR spectra of (a) original fibers, carboxymethylated cellulose fibers, and Sul-CNCs, as well as (b) Car-CNCs under different APS oxidation times. XRD images of (c) original fibers, CMC-COONa, and Sul-CNCs, as well as (d) Car-CNCs prepared under different APS oxidation times. TGA and DTG images of (e) original fibers, CMC-COONa, and Sul-CNCs, as well as (f) Car-CNCs under different APS oxidation times.

disordered and partially ordered domains of native cellulose were both disrupted to a varying extent. Compared with the crystalline region, the amorphous region of cellulose is looser and has a larger molecular distance; thereby, it can be readily accessible by the reactants and destroyed effectively.[38,42] Subsequently, when the carboxymethylated slurry was exposed to the APS system, balloon-like structures would play a crucial role to improve production efficiency. As shown in Figure 1h, persulfate (HSO_4^-), peroxide free radicals ($SO_4^{\cdot-}$), and hydrogen peroxide (H_2O_2) were generated during the APS oxidation process. $SO_4^{\cdot-}$ free radicals and H_2O_2 could penetrate balloon-like structures readily, oxidate the rest C_6 hydroxyl groups to the carboxyl groups, and form stronger electrostatic repulsion between fibrils, resulting in the rapid formation of Car-CNCs under mild conditions. Therefore, owing to the swelling of carboxymethylation, the oxidation time of APS reduced significantly.

3.2. Morphology, Dimensions, Yields, and Zeta Potentials of Cellulose Nanocrystals. After carboxymethylation pretreatment, we further studied the effects of APS oxidation time, reaction temperature, and APS concentration on the morphology, dimensions, yields, and zeta potentials of Car-CNCs. For comparison, the nanocrystal suspension with sulfate half-ester groups (Sul-CNCs) was also investigated. The

https://doi.org/10.1021/acsomega.2c08239
ACS Omega 2023, 8, 15114−15123

detailed data were summarized in Table S1 and the inset of AFM images.

As shown in Figure 2, the obtained Car-CNCs and Sul-CNCs exhibited typical structures with a nano-scale length and diameter, suggesting we have successfully prepared the individual CNCs. AFM images were analyzed using ImageJ V. 1.8.0 software to investigate the morphological features and dimensions of cellulose nanocrystals (Figures S4−5). Under 45 °C and 70 min, the average length and width of obtained Sul-CNCs were 118.2 ± 55.5 and 17.9 ± 3.0 nm (Table S1), respectively. While the morphology and dimension of Car-CNCs were strongly affected by extraction conditions. The average width of Car-CNCs ranged from 11.4 to 18.4 nm, and the corresponding average lengths ranged from 74.8 to 145.3 nm. An obvious downward trend was observed in the average length with the increasing oxidation time from 15 to 120 min (under 0.5 M and 70 °C), reaction temperature from 50 to 90 °C (under 0.5 M and 30 min), and APS concentration from 0.25 to 1.0 M (under 70 °C and 30 min) (Table S1 and the inset of AFM images). The successive decrease in the length of Car-CNCs was mainly due to the constant breakdown of disordered or even crystalline domains by hydrolyzing the 1,4-β-glycosidic bonds of the cellulose chains during APS oxidation.

The yields of Car-CNCs and Sul-CNCs were calculated by eq S1 and the results were summarized in the inset of AFM images and Table S1. Interestingly, the as-prepared Sul-CNCs exhibited the lowest yield, suggesting that a large number of cellulose chains were degraded under harsh sulfuric acid.[43] On the contrary, the yields of as-prepared Car-CNCs by our milder APS oxidation were all higher than that of Sul-CNCs. Moreover, with the increasing of reaction time, the yield increased first and then decreased. When the reaction time was 30 min, it had the maximum value. Due to the short reaction time (less than 30 min), CNCs were not fully extracted, and large unreacted fibers remained in the reaction system. When the reaction time was prolonged than 30 min, the reaction intensity was excessive, and the isolated CNCs were degraded during constant oxidation. Similar trends were also observed with the increasing of reaction temperature or APS concentration. It was worth noting when the oxidation time was 30 min, APS concentration was 0.5 mol L^{-1}, and reaction temperature was 70 °C, the Car-CNCs-30 min has the highest yield of 60.6%. Obviously, the carboxymethylation swelling pretreatment not only shortened the oxidation time of APS but also kept a high yield. Besides, these results also demonstrated carboxymethylation collaborative APS oxidation was superior to the previously reported conventional APS oxidation approaches (Table S2).

In addition, the zeta potential was also investigated to evaluate the dispersion of Car-CNC and Sul-CNC suspensions. Generally, a higher absolute zeta potential value shows a more stable dispersion due to electrostatic repulsion.[27] As displayed in the inset of AFM images and Table S1, the Sul-CNCs showed the lowest zeta potential value (−51.3 mV), which is associated with the abundant sulfate groups. As for Car-CNCs, after carboxymethylation pretreatment, native cellulose fibers converted to CMC-COONa with the zeta potential decreasing from −15.6 to −37.6 mV, indicating the −OH groups of C_2, C_3, and C_6 positions on the cellulose surface partly converted to −COONa groups. Furthermore, when the APS oxidation temperature was lower than 80 °C or the reaction time was less than 90 min, the zeta potential of the Car-CNCs showed a higher value than that of CMC-COONa. This phenomenon could be relevant to the electronegativity of −COOH and −COONa groups. In the suspension, −COONa groups were completely ionized to $-COO^-$ and sodium ion hydrate, which would increase the electrostatic repulsive force between the cellulose chains. However, the −COOH groups were partially ionized to $-COO^-$ and H^+, which would restrict the electrostatic balance among cellulose chains.[44] On the contrary, as the temperature was above 80 °C or reaction time was prolonged to 120 min, the zeta potential of Car-CNCs decreased significantly and was lower than CMC-COONa. That's because excessive oxidation would enhance the amount of −COOH groups and provide stronger electrostatic repulsion force.

3.3. Chemical Structure Analysis. The chemical structures of the raw fibers, CMC-COONa, Car-CNCs, and Sul-CNCs were confirmed by the FT-IR spectra. As shown in Figure 3a,b, all samples exhibited similar characteristic peaks at ≈3400, 2900, and 1060 cm^{-1}, which corresponded to the O−H stretching, C−H vibration, and C−O−C pyranose ring stretching vibration in cellulose, respectively. These results indicated the crystal structures of CMC-COONa, Car-CNCs, and Sul-CNCs were not changed after carboxymethylation, APS oxidation, and sulfuric acid hydrolysis, respectively. Compared with the original fibers, a new peak that occurred at ≈1600 cm^{-1} was found in the spectra of carboxymethylated cellulose slurry (Figure 3a), which corresponded to the C═O stretching of sodium carboxylate groups. The results indicated that part hydroxyl groups at the C_6, C_2, and C_3 positions successfully converted to the sodium carboxylate groups. However, after APS oxidation, the intensity of C═O absorption peak at 1600 cm^{-1} disappeared and red-shifted to the peak at ≈1737 cm^{-1} (Figures 3b and S6a,b), which could be attributed to that the sodium carboxylate groups were all converted to free carboxyl groups and part of the rest unreacted primary alcohol groups on C_6 position were selectively oxidized to carboxyl groups.[9] For the case of Sul-CNCs, a new band at 1202 cm^{-1} could be also observed in Figure 3a, suggesting the introduction of sulfate groups. Thus, these characteristic peaks demonstrated the successful isolation of cellulose nanocrystals from the original bleached softwood fibers.

3.4. Crystallinity Analysis. The XRD measurement was performed to evaluate the crystal structure and crystallinity of the raw fibers, CMC-COONa, Car-CNCs, and Sul-CNCs. As shown in Figures 3c,d and S6c,d, all samples exhibited similar diffraction peaks at around 2θ = 14.9, 16.5, 22.7, and 34.6°, which were corresponding to the 1−10, 110, 200, and 004 crystal planes of cellulose I_β, respectively, suggesting the crystal structure of cellulose did not change after carboxymethylation, APS oxidation, and sulfuric acid hydrolysis,[4] respectively. The crystallinity index (CrI) is a key factor that affects the mechanical and thermal properties of the cellulose samples, which can be calculated by eq S2.

As shown in Table S3, the CrI of original native fibers is 73.4%. After treating the native fibers by carboxymethylation, we observed a significant decrease in the crystallinity of CMC-COONa (61.1%). The results indicated carboxymethylation and mechanical shear stress in the swelling process were nonselective and might destroy both amorphous and crystalline regions of cellulose. For Car-CNCs, however, all their CrI (65.8−74.9%) values were higher than those of CMC-COONa (61.1%) (Table S3), which was ascribed to the

https://doi.org/10.1021/acsomega.2c08239
ACS Omega 2023, 8, 15114−15123

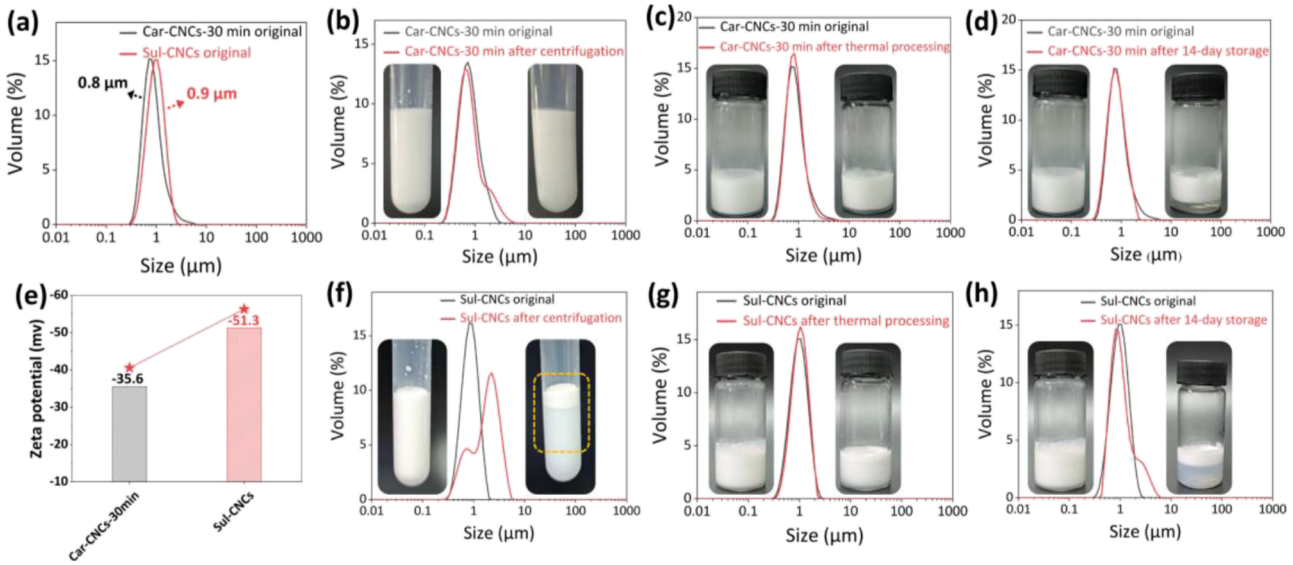

Figure 4. Droplet size distributions of (a) freshly prepared emulsions stabilized by Car-CNCs and Sul-CNCs, as well as (b−d) Car-CNC-based emulsions before and after (b) centrifugation, (c) thermal processing, and (d) 14 days of storage. (e) Zeta potentials of the Car-CNCs and Sul-CNCs. Droplet size distributions of the Sul-CNC-based emulsions before and after (f) centrifugation, (g) thermal processing, and (h) 14 days of storage. Insets are the optical photos of the emulsions.

further decomposition of amorphous regions of carboxymethylated cellulose fibers during APS oxidation. In addition, we also observed an increase in CrI for Sul-CNCs (82.5%) compared to the original fibers (73.4%), which was mainly attributed to that the hydronium ions could penetrate into the more accessible amorphous regions and promote the hydrolytic cleavage of glycosidic bonds, thereby liberating the individual crystallites.[45]

With the increasing oxidation time from 15 to 120 min, the CrI of Car-CNCs gradually increased from ≈70 to 74.9%, and then decreased to 70.2% (Figure 3d and Table S3). That's because the disordered domains of cellulose mainly conducted sufficient decomposition within 90 min, while the crystalline regions might be partially destroyed as the reaction time was further prolonged (120 min).[9,18] When the APS concentration increased from 0.25 to 1.0 mol L^{-1}, the CrI of Car-CNCs increased from 69.3 to 72.4% (Table S3 and Figure S6c), attributed to the large decomposition of amorphous regions of cellulose. Moreover, the effect of oxidation temperature on crystallinity is similar to that of the oxidation time, where the CrI of Car-CNCs increased from 65.8 to 73.2% and then decreased to 71.7% with the increasing temperatures from 50 to 90 °C (Table S3 and Figure S6d). These results demonstrated that the CrI was not only affected by the isolation approaches but also the isolation conditions.

3.5. Thermal Stability. Figures 3e,f and S6e,f show TG curves of the raw fibers, CMC-COONa, Car-CNCs prepared under different oxidation conditions, and Sul-CNCs obtained from acid hydrolysis. With the temperature ranging from 40 to 120 °C, we observed an initial weight loss (3−9%). The weight loss at this stage was owing to the vaporization of the moisture that existed in the cellulose fibrils; the curve differences of samples were caused by different initial moisture contents.[46] The main weight loss occurred in temperatures from 200 to 400 °C, which was owing to the thermal degradation of cellulose.[4] The thermal properties (including the onset and maximum degradation temperatures (T_{onset} and T_{max}) and residual mass) are also listed in Table S3. Compared with original fibers (T_{onset} = 330.9 °C), carboxymethylated cellulose fibers degraded at a lower initial temperature of T_{onset} = 287.3 °C, which was owing to the introduction of −COONa groups.[39]

In addition, T_{onset} (319.5 °C, 291.7 °C) and T_{max} (346.6 °C, 330 °C) of Car-CNCs-50 °C and Car-CNCs-60 °C, respectively, were higher than that of CMC-COONa (T_{onset} = 287.3 °C, T_{max} = 307.1 °C) (Table S3 and Figure 3f). This result could be attributed to the fact that −COONa groups have completely converted to −COOH groups under mild conditions. In addition, the cellulose nanocrystals with −COOH groups were more stable than those with $-COONa^+$ groups.[23] However, as the APS concentration, oxidation time, and reaction temperature further increased, the thermal stability of Car-CNCs decreased and was lower than CMC-COONa. One reason could be owing to the smaller fiber dimensions (length and diameter) as compared to the macroscopic carboxymethylated slurry. Another reason was that the fiber dimensions became smaller with the increasing intensity of APS oxidation, which would lead to higher surface areas exposed to heat.[21] Fortunately, our Car-CNCs all retained high thermal stability until 250 °C, which can satisfy the general processing temperature (above 200 °C) in thermoplastic applications.[11] Nevertheless, Sul-CNCs using sulfuric acid hydrolysis tended to decompose when the temperature was only ≈191.2 °C,[47] which were easier degraded than our samples at a high temperature.

More importantly, when at the oxidation condition (at 0.5 mol L^{-1}, 50 °C, and 30 min), the Car-CNCs exhibited the highest thermal stability. Its T_{onset} and T_{max} could be as high as 319.5 and 346.6 °C, respectively, which was better than other reported CNCs that were prepared directly using APS oxidation.[9,18]

3.6. Pickering Emulsion Stability. Recently, oil-in-water emulsions (O/W) have attracted more attention in many fields (such as food science, cosmetics, energy storage, etc.), due to their immiscible systems of oil droplets in the water phase. Pickering emulsions stabilized by cellulose-based particles have

https://doi.org/10.1021/acsomega.2c08239
ACS Omega 2023, 8, 15114−15123

been widely reported, especially, CNCs have been proven very efficient in stabilizing oil/water interfaces. Compared with other conventional emulsifiers, CNCs are biocompatible, biodegradable, sustainable, nontoxic, rigid, and hydrophilic.[48,49] Although the Pickering emulsions stabilized by CNCs were very effective, they could destabilize when subjected to a changeable environment. The stabilities of emulsions were strongly dependent on the different shapes, sizes, or surface charges of CNCs and emulsion viscosity, etc.[50−53] In this study, to investigate CNCs' emulsifying abilities, Car-CNCs (selecting Car-CNCs-30 min) and Sul-CNCs were used as stabilizers, and liquid paraffin (LP) was chosen as the oil phase to prepare oil-in-water emulsions. The emulsion stability (ES) was evaluated from three aspects: physical stability, thermal stability, and storage stability.

As shown in Figure S7a,e, the pickering emulsions stabilized by Car-CNCs and Sul-CNCs showed almost similar droplet sizes. The surface-weighted mean diameters ($D_{(3,2)}$) of them were ≈0.8 and ≈0.9 μm (Figure 4a and Table S4), respectively. This phenomenon could be associated with the almost similar CNCs size (Car-CNCs: L = 118.1 ± 43.4 nm, D = 14.2 ± 3.1 nm, and an aspect ratio of 9.2 ± 2.1; Sul-CNCs: L = 118.2 ± 55.5 nm, D = 17.9 ± 3.0 nm, and an aspect ratio of 8.2 ± 1.9)[27,54](the inset of Figure S8a,b) and the identical CNCs loadings.[53] Moreover, the surface coverage of the droplets was calculated according to eq S4, which were 81.8% for Car-CNC-based emulsions and 48.7% for Sul-CNC-based emulsions, respectively. The higher surface coverage of Car-CNC-based emulsions than Sul-CNC-based emulsions indicated that the Car-CNCs had better emulsifying properties. It may be due to the lower zeta potential of Sul-CNCs (−51.3 mV) than Car-CNCs (−35.6 mV), which results in stronger electrostatic repulsion and prevents CNCs partitioning to the oil−water interface (Figure S8c).[55−57] Additionally, we also measured the molar surface charges of Sul-CNCs and Car-CNCs by conductometric titration according to previously reported methods,[58] as shown in Figure S9. The consumed volume of NaOH solution for Sul-CNCs was about 2.6 mL, which was higher than that of Car-CNCs (≈1.5 mL). The results exhibited molar surface charges of Sul-CNCs were much higher than that of Car-CNCs, which could form stronger electrostatic repulsion between Sul-CNC particles and affect the ES adversely. Thus, the conclusion drawn from the conductometric titration test was consistent with the above-measured Zeta potential.

Emulsion physical stability. We used centrifugation to assess the physical stability of the emulsions. Centrifugation could speed up the creaming process, concentrate the droplets by excluding excess water from the emulsions and create a closed-pack emulsion.[59] After the centrifugation process, the ES value of the emulsions was calculated by eq S5, which were 100% for Car-CNC-based emulsions and 21.1% for Sul-CNC-based emulsions, respectively (Table S4). These results demonstrated that the emulsions stabilized by Car-CNCs were more stable than Sul-CNC-based emulsions. As shown in Figures 4b,f, S7a,b,e,f, and Table S4, there was no emulsion coalescence/separation, and few changes of droplet size and size distribution were found in the Car-CNC-based emulsions before and after centrifugation. However, Sul-CNC-based emulsions showed an increase in emulsion size, a large variation in droplet size distribution, and large-scale phase separation after centrifugation. These phenomena may be associated with low surface coverage of droplets. Sul-CNCs with a lower zeta potential (that is, a higher charge density) could induce detrimental electrostatic repulsions and prevent CNCs from being absorbed in oil/water interfaces, resulting in poor surface coverage.[60] The droplets with a low and insufficient surface coverage could be more prone to coalesce and destabilize when subjected to centrifugation.[61−64]

Emulsion thermal stability. As shown in Figures 4, S7, and Table S4, there were almost no changes in droplet size and size distribution found in all as-prepared emulsions. The ES values of Car-CNC-based and Sul-CNC-based emulsions were both 100%. These results suggested that all as-prepared emulsions could be well resistant to thermal processing. It was due to the temperature might not have a major influence on the strong steric or electrostatic repulsion between the emulsion particles.[65]

Emulsion storage stability. After 14 days of storage, the ES value, droplet size, and size distribution of emulsions were measured. The corresponding data are presented in Table S4, Figures 4, and S7. The Car-CNC-based emulsions showed almost no variation in emulsion size, size distribution, or morphology, although the oil creaming phase and aqueous phase stratified. In general, an emulsion can be considered stable as long as no coalescence occurs; that means the size and size distribution should not change.[59] The stratification was mainly due to the effect of gravity and the different densities between LP and water during long-term storage[66,67] (0.835 g/cm^3 for LP and 1.0 g/cm^3 for the water). Besides, a similar stratification phenomenon was also observed in the Sul-CNC stabilized emulsions. However, Sul-CNC-based emulsions showed an increase in droplet size distribution and particle size after 14 days of storage.

Medium viscosity has also been found one-factor affecting ES.[68] We further measured the viscosity of the emulsions prepared by Sul-CNCs and Car-CNCs. As shown in Figure S10, the freshly prepared emulsions based on Sul-CNC and Car-CNC displayed almost similar viscosities, primarily due to the similar morphologies of CNCs, identical quantities of CNCs, and the same amounts of LP in emulsions.[53,66] Interestingly, our above experimental results demonstrate that Sul-CNC-based emulsions possessed weaker stability than Car-CNC-based emulsions. It was obvious that viscosity had little effect on the ES in our system.

However, the two emulsions exhibited different trends in viscosity change after storage for 5 days. Car-CNC-based emulsions retained almost the same viscosity as the original emulsions, while Sul-CNC-based emulsions decreased greatly compared with freshly prepared Sul-CNC-based emulsions. A decrease in viscosity after long-term storage might be caused by lamination and demulsification due to insufficient surface coverage. The results showed that Sul-CNCs and Car-CNCs did not affect the viscosity of fresh emulsions in our system, but their different zeta potentials affected their long-term stability.

Above all, the Car-CNC-based emulsions show excellent stability and can withstand centrifugation, thermal processing, and long-term storage, superior to the Sul-CNC-based emulsions. Therefore, the pickering emulsions stabilized by our Car-CNCs could offer promising potentials in practical applications such as thermal energy storage, food science, the cosmetic industry, etc.

https://doi.org/10.1021/acsomega.2c08239
ACS Omega 2023, 8, 15114−15123

4. CONCLUSIONS

In this study, we developed a high-efficient and scalable method for preparing Car-CNCs by carboxymethylation pretreatment-assisted APS oxidation. As expected, the carboxymethylation pretreatment facilitates the swelling of wood cell walls and exposed more C_6 hydroxy groups, thus improving the APS oxidation efficiency and shortening the preparation time from 16−24 h to only ≈30 min. Moreover, we can adjust the yield, micromorphology, crystallinity, and thermal stability of Car-CNCs by controlling different APS oxidation conditions. Among them, the Car-CNCs-30 min exhibited a maximum yield of 60.6% with an average length of 118.1 ± 43.4 nm and diameter of 14.2 ± 3.1 nm. More importantly, the yield, thermal stability, and the preparation efficiency of our Car-CNCs were superior to the conventional CNCs prepared from sulfuric acid hydrolysis and conventional APS oxidation. Therefore, our two-step collaborative process offered a promising and economical strategy for preparing CNCs on a large scale. Additionally, our Car-CNCs also demonstrated excellent stabilization for Pickering emulsion preparation, which has promising potential in numerous fields.

■ ASSOCIATED CONTENT

Supporting Information

The Supporting Information is available free of charge at https://pubs.acs.org/doi/10.1021/acsomega.2c08239.

Characterization and methods; images of the reactor and CMC-COONa slurry; size distributions of the raw fibers and CMC-COONa; microscopic images of the CMC-COONa; size distributions, FT-IR, XRD, TGA, and DTG results of the Car-CNCs; microscopic morphologies of the Car-CNC-based and Sul-CNC-based emulsions; AFM images of the CNCs; schematic illustrations of the emulsion stability with different CNCs; conductometric titration curves of the Car-CNCs and Sul-CNCs; and flow curves of the emulsions (PDF)

■ AUTHOR INFORMATION

Corresponding Authors

Yuan Wei − *State Key Laboratory of Pulp and Paper Engineering, College of Light Industry and Engineering and Guangdong Engineering Technology Research and Development Center of Specialty Paper and Paper-Based Functional Materials, South China University of Technology, Guangzhou 510640, China*; Email: wyuan_1122@163.com

Yangyang Qian − *State Key Laboratory of Pulp and Paper Engineering, College of Light Industry and Engineering and Guangdong Engineering Technology Research and Development Center of Specialty Paper and Paper-Based Functional Materials, South China University of Technology, Guangzhou 510640, China; College of Tea (Pu'er), West Yunnan University of Applied Sciences, Pu'er 665000, China*; Email: qian6yang@163.com

Gang Chen − *State Key Laboratory of Pulp and Paper Engineering, College of Light Industry and Engineering and Guangdong Engineering Technology Research and Development Center of Specialty Paper and Paper-Based Functional Materials, South China University of Technology, Guangzhou 510640, China*; orcid.org/0000-0003-3886-0199; Email: papercg@scut.edu.cn

Authors

Yikang Liu − *State Key Laboratory of Pulp and Paper Engineering, College of Light Industry and Engineering and Guangdong Engineering Technology Research and Development Center of Specialty Paper and Paper-Based Functional Materials, South China University of Technology, Guangzhou 510640, China*

Yingying He − *State Key Laboratory of Pulp and Paper Engineering, College of Light Industry and Engineering and Guangdong Engineering Technology Research and Development Center of Specialty Paper and Paper-Based Functional Materials, South China University of Technology, Guangzhou 510640, China*

Chunyu Wang − *State Key Laboratory of Pulp and Paper Engineering, College of Light Industry and Engineering and Guangdong Engineering Technology Research and Development Center of Specialty Paper and Paper-Based Functional Materials, South China University of Technology, Guangzhou 510640, China*

Complete contact information is available at: https://pubs.acs.org/10.1021/acsomega.2c08239

Author Contributions

Y.L.: Methodology, Investigation, Formal analysis, Writing - original draft. Y.W.: Methodology, Investigation, Formal analysis, Data curation, Writing - review & editing. Y.H.: Formal analysis, Data curation. Y.Q.: Investigation, Data curation, Writing - review & editing. C.W.: Methodology, Data curation. G.C.: Resources, Funding acquisition, Project administration, Supervision, Writing - review & editing.

Notes

The authors declare no competing financial interest.

■ ACKNOWLEDGMENTS

The photographs in Figures 1, and 4, and TOC were taken by the author Y.L. The authors acknowledge the National Key Research and Development Program of China (no. 2018YFC1902102), the State Key Laboratory of Pulp and Paper Engineering at South China University of Technology (no. 2020ZD02), and the Basic and Applied Basic Research Foundation of Guangdong Province of China (no. 2021A1515010538). Y.W. acknowledges the financial support of the China Scholarship Council (202106150089).

■ REFERENCES

(1) Rajinipriya, M.; Nagalakshmaiah, M.; Robert, M.; Elkoun, S. Importance of Agricultural and Industrial Waste in the Field of Nanocellulose and Recent Industrial Developments of Wood Based Nanocellulose: A Review. *ACS Sustainable Chem. Eng.* **2018**, *6*, 2807−2828.

(2) Dufresne, A. Nanocellulose: a new ageless bionanomaterial. *Mater. Today* **2013**, *16*, 220−227.

(3) Liu, W.; Liu, K.; Du, H.; Zheng, T.; Zhang, N.; Xu, T.; Pang, B.; Zhang, X.; Si, C.; Zhang, K. Cellulose Nanopaper: Fabrication, Functionalization, and Applications. *Nanomicro Lett.* **2022**, *14*, 104.

(4) Oun, A. A.; Rhim, J.-W. Characterization of carboxymethyl cellulose-based nanocomposite films reinforced with oxidized nanocellulose isolated using ammonium persulfate method. *Carbohydr. Polym.* **2017**, *174*, 484−492.

(5) Xu, X.; Liu, F.; Jiang, L.; Zhu, J. Y.; Haagenson, D.; Wiesenborn, D. P. Cellulose Nanocrystals vs. Cellulose Nanofibrils: A Comparative Study on Their Microstructures and Effects as Polymer Reinforcing Agents. *ACS Appl. Mater. Interfaces* **2013**, *5*, 2999−3009.

(6) Zhu, H.; Luo, W.; Ciesielski, P. N.; Fang, Z.; Zhu, J. Y.; Henriksson, G.; Himmel, M. E.; Hu, L. Wood-Derived Materials for Green Electronics, Biological Devices, and Energy Applications. *Chem. Rev.* **2016**, *116*, 9305−9374.
(7) Cheng, S.; Zhang, Y.; Cha, R.; Yang, J.; Jiang, X. Water-soluble nanocrystalline cellulose films with highly transparent and oxygen barrier properties. *Nanoscale* **2016**, *8*, 973−978.
(8) Dai, L.; Wang, Y.; Zou, X.; Chen, Z.; Liu, H.; Ni, Y. Ultrasensitive Physical, Bio, and Chemical Sensors Derived from 1-, 2-, and 3-D Nanocellulosic Materials. *Small* **2020**, *16*, No. 1906567.
(9) Khanjanzadeh, H.; Park, B.-D. Optimum oxidation for direct and efficient extraction of carboxylated cellulose nanocrystals from recycled MDF fibers by ammonium persulfate. *Carbohydr. Polym.* **2021**, *251*, No. 117029.
(10) Mahmoud, K. A.; Male, K. B.; Hrapovic, S.; Luong, J. H. T. Cellulose Nanocrystal/Gold Nanoparticle Composite as a Matrix for Enzyme Immobilization. *ACS Appl. Mater. Interfaces* **2009**, *1*, 1383−1386.
(11) Mascheroni, E.; Rampazzo, R.; Ortenzi, M. A.; Piva, G.; Bonetti, S.; Piergiovanni, L. Comparison of cellulose nanocrystals obtained by sulfuric acid hydrolysis and ammonium persulfate, to be used as coating on flexible food-packaging materials. *Cellulose* **2016**, *23*, 779−793.
(12) Yang, H.; Tejado, A.; Alam, N.; Antal, M.; van de Ven, T. G. M. Films Prepared from Electrosterically Stabilized Nanocrystalline Cellulose. *Langmuir* **2012**, *28*, 7834−7842.
(13) Lin, N.; Huang, J.; Dufresne, A. Preparation, properties and applications of polysaccharide nanocrystals in advanced functional nanomaterials: a review. *Nanoscale* **2012**, *4*, 3274−3294.
(14) Liu, Y.; Guo, B.; Xia, Q.; Meng, J.; Chen, W.; Liu, S.; Wang, Q.; Liu, Y.; Li, J.; Yu, H. Efficient Cleavage of Strong Hydrogen Bonds in Cotton by Deep Eutectic Solvents and Facile Fabrication of Cellulose Nanocrystals in High Yields. *ACS Sustainable Chem. Eng.* **2017**, *5*, 7623−7631.
(15) Zhao, D.; Pang, B.; Zhu, Y.; Cheng, W.; Cao, K.; Ye, D.; Si, C.; Xu, G.; Chen, C.; Yu, H. A Stiffness-Switchable, Biomimetic Smart Material Enabled by Supramolecular Reconfiguration. *Adv. Mater.* **2022**, *34*, No. e2107857.
(16) Jiang, G.; Wang, G.; Zhu, Y.; Cheng, W.; Cao, K.; Xu, G.; Zhao, D.; Yu, H. A Scalable Bacterial Cellulose Ionogel for Multisensory Electronic Skin. *Research* **2022**, *2022*, No. 9814767.
(17) Goh, K. Y.; Ching, Y. C.; Chuah, C. H.; Abdullah, L. C.; Liou, N. Individualization of microfibrillated celluloses from oil palm empty fruit bunch: comparative studies between acid hydrolysis and ammonium persulfate oxidation. *Cellulose* **2016**, *23*, 2245−2246.
(18) Bashar, M. M.; Zhu, H.; Yamamoto, S.; Mitsuishi, M. Highly carboxylated and crystalline cellulose nanocrystals from jute fiber by facile ammonium persulfate oxidation. *Cellulose* **2019**, *26*, 3671−3684.
(19) Castro-Guerrero, C. F.; Gray, D. G. Chiral nematic phase formation by aqueous suspensions of cellulose nanocrystals prepared by oxidation with ammonium persulfate. *Cellulose* **2014**, *21*, 2567−2577.
(20) Jiang, F.; Han, S.; Hsieh, Y.-L. Controlled defibrillation of rice straw cellulose and self-assembly of cellulose nanofibrils into highly crystalline fibrous materials. *RSC Adv.* **2013**, *3*, 12366−12375.
(21) Jiang, F.; Hsieh, Y.-L. Chemically and mechanically isolated nanocellulose and their self-assembled structures. *Carbohydr. Polym.* **2013**, *95*, 32−40.
(22) Leung, A. C. W.; Hrapovic, S.; Lam, E.; Liu, Y.; Male, K. B.; Mahmoud, K. A.; Luong, J. H. T. Characteristics and Properties of Carboxylated Cellulose Nanocrystals Prepared from a Novel One-Step Procedure. *Small* **2011**, *7*, 302−305.
(23) Lam, E.; Leung, A. C. W.; Liu, Y.; Majid, E.; Hrapovic, S.; Male, K. B.; Luong, J. H. T. Green Strategy Guided by Raman Spectroscopy for the Synthesis of Ammonium Carboxylated Nanocrystalline Cellulose and the Recovery of Byproducts. *ACS Sustainable Chem. Eng.* **2013**, *1*, 278−283.
(24) Haunreiter, K. J.; Dichiara, A. B.; Gustafson, R. Nanocellulose by Ammonium Persulfate Oxidation: An Alternative to TEMPO-Mediated Oxidation. *ACS Sustainable Chem. Eng.* **2022**, *10*, 3882−3891.
(25) Filipova, I.; Fridrihsone, V.; Cabulis, U.; Berzins, A. Synthesis of Nanofibrillated Cellulose by Combined Ammonium Persulphate Treatment with Ultrasound and Mechanical Processing. *Nanomaterials* **2018**, *8*, 640.
(26) Marwanto, M.; Maulana, M. I.; Febrianto, F.; Wistara, N. J.; Nikmatin, S.; Masruchin, N.; Zaini, L. H.; Lee, S.; Kim, N. Effect of Oxidation Time on the Properties of Cellulose Nanocrystals Prepared from Balsa and Kapok Fibers Using Ammonium Persulfate. *Polymer* **2021**, *13*, 13.
(27) Zhang, H.; Chen, Y.; Wang, S.; Ma, L.; Yu, Y.; Dai, H.; Zhang, Y. Extraction and comparison of cellulose nanocrystals from lemon (Citrus limon) seeds using sulfuric acid hydrolysis and oxidation methods. *Carbohydr. Polym.* **2020**, *238*, No. 116180.
(28) Wang, H.; Pudukudy, M.; Ni, Y.; Zhi, Y.; Zhang, H.; Wang, Z.; Jia, Q.; Shan, S. Synthesis of nanocrystalline cellulose via ammonium persulfate-assisted swelling followed by oxidation and their chiral self-assembly. *Cellulose* **2020**, *27*, 657−676.
(29) Liu, Y.; Liu, L.; Wang, K.; Zhang, H.; Yuan, Y.; Wei, H.; Wang, X.; Duan, Y.; Zhou, L.; Zhang, J. Modified ammonium persulfate oxidations for efficient preparation of carboxylated cellulose nanocrystals. *Carbohydr. Polym.* **2020**, *229*, No. 115572.
(30) He, J.; Bian, K.; Piao, G. Self-assembly properties of carboxylated tunicate cellulose nanocrystals prepared by ammonium persulfate oxidation and subsequent ultrasonication. *Carbohydr. Polym.* **2020**, *249*, No. 116835.
(31) Zhang, K.; Sun, P.; Liu, H.; Shang, S.; Song, J.; Wang, D. Extraction and comparison of carboxylated cellulose nanocrystals from bleached sugarcane bagasse pulp using two different oxidation methods. *Carbohydr. Polym.* **2016**, *138*, 237−243.
(32) Cheng, M.; Qin, Z.; Liu, Y.; Qin, Y.; Li, T.; Chen, L.; Zhu, M. Efficient extraction of carboxylated spherical cellulose nanocrystals with narrow distribution through hydrolysis of lyocell fibers by using ammonium persulfate as an oxidant. *J. Mater. Chem. A* **2014**, *2*, 251−258.
(33) Isogai, A.; Saito, T.; Fukuzumi, H. TEMPO-oxidized cellulose nanofibers. *Nanoscale* **2011**, *3*, 71−85.
(34) Wågberg, L.; Decher, G.; Norgren, M.; Lindström, T.; Ankerfors, M.; Axnäs, K. The Build-Up of Polyelectrolyte Multilayers of Microfibrillated Cellulose and Cationic Polyelectrolytes. *Langmuir* **2008**, *24*, 784−795.
(35) Filipova, I.; Serra, F.; Tarrés, Q.; Mutjé, P.; Delgado-Aguilar, M. Oxidative treatments for cellulose nanofibers production: a comparative study between TEMPO-mediated and ammonium persulfate oxidation. *Cellulose* **2020**, *27*, 10671−10688.
(36) Kono, H.; Tsukamoto, E.; Tajima, K. Facile Post-Carboxymethylation of Cellulose Nanofiber Surfaces for Enhanced Water Dispersibility. *ACS Omega* **2021**, *6*, 34107−34114.
(37) Saito, T.; Nishiyama, Y.; Putaux, J.-L.; Vignon, M.; Isogai, A. Homogeneous Suspensions of Individualized Microfibrils from TEMPO-Catalyzed Oxidation of Native Cellulose. *Biomacromolecules* **2006**, *7*, 1687−1691.
(38) Sim, G.; Alam, M. N.; Godbout, L.; van de Ven, T. Structure of swollen carboxylated cellulose fibers. *Cellulose* **2014**, *21*, 4595−4606.
(39) Lei, C.; Wei, Y.; Qian, Y.; Wang, Q.; Zhu, P.; Qiu, G.; Chen, G. Large-Scale Manufacture of Recyclable Bioplastics from Renewable Cellulosic Biomass Derived from Softwood Kraft Pulp. *ACS Appl. Polym. Mater.* **2022**, *4*, 1334−1343.
(40) Bano, S.; Negi, Y. S. Studies on cellulose nanocrystals isolated from groundnut shells. *Carbohydr. Polym.* **2017**, *157*, 1041−1049.
(41) Xing, L.; Hu, C.; Zhang, W.; Guan, L.; Gu, J. Transition of cellulose supramolecular structure during concentrated acid treatment and its implication for cellulose nanocrystal yield. *Carbohydr. Polym.* **2020**, *229*, No. 115539.
(42) Sim, G.; van de Ven, T. G. M. The S3 layer isolated from carboxymethylated cellulose wood fibers. *Cellulose* **2015**, *22*, 45−52.

https://doi.org/10.1021/acsomega.2c08239
ACS Omega 2023, 8, 15114−15123

(43) Xiao, Y.; Liu, Y.; Wang, X.; Li, M.; Lei, H.; Xu, H. Cellulose nanocrystals prepared from wheat bran: Characterization and cytotoxicity assessment. *Int. J. Biol. Macromol.* **2019**, *140*, 225−233.
(44) Qian, Y.; Liu, Y.; Zhang, Y.; Lei, C.; Lin, L.; Chen, G. Protonation and dip-coating synergistically enhancing dimensional stability of multifunctional cellulose-based films. *Cellulose* **2022**, *29*, 967−983.
(45) Li, R.; Fei, J.; Cai, Y.; Li, Y.; Feng, J.; Yao, J. Cellulose whiskers extracted from mulberry: A novel biomass production. *Carbohydr. Polym.* **2009**, *76*, 94−99.
(46) Oun, A. A.; Rhim, J.-W. Preparation and characterization of sodium carboxymethyl cellulose/cotton linter cellulose nanofibril composite films. *Carbohydr. Polym.* **2015**, *127*, 101−109.
(47) Kargarzadeh, H.; Ahmad, I.; Abdullah, I.; Dufresne, A.; Zainudin, S. Y.; Sheltami, R. M. Effects of hydrolysis conditions on the morphology, crystallinity, and thermal stability of cellulose nanocrystals extracted from kenaf bast fibers. *Cellulose* **2012**, *19*, 855−866.
(48) Kasiri, N.; Fathi, M. Production of cellulose nanocrystals from pistachio shells and their application for stabilizing Pickering emulsions. *Int. J. Biol. Macromol.* **2018**, *106*, 1023−1031.
(49) Wang, Y.; Zhao, W.; Han, M.; Guan, L.; Han, L.; Hemraj, A.; Tam, K. C. Sustainable Superhydrophobic Surface with Tunable Nanoscale Hydrophilicity for Water Harvesting Applications. *Angew. Chem., Int. Ed.* **2022**, *134*, No. e202115238.
(50) Dai, H. J.; Wu, J. H.; Zhang, H.; Chen, Y.; Ma, L.; Huang, H. H.; Huang, Y.; Zhang, Y. H. Recent advances on cellulose nanocrystals for Pickering emulsions: Development and challenge. *Trends Food Sci. Technol.* **2020**, *102*, 16−29.
(51) Feng, X.; Dai, H. J.; Fu, Y.; Yu, Y.; Zhu, H. K.; Wang, H. X.; Chen, H.; Ma, L.; Zhang, Y. H. Regulation mechanism of nanocellulose with different morphologies on the properties of low-oil gelatin emulsions: Interfacial adsorption or network formation? *Food Hydrocolloids* **2022**, *133*, No. 107960.
(52) Chen, L. D.; Lin, C. H.; Ye, Q.; Chen, J. Q.; Chen, Z. H.; Jiang, J. H.; Zhou, M. L.; Li, J. H.; Hu, K. H.; Sun, S. J. A fungal cellulose nanocrystals-based approach to improve the stability of triterpenes loaded Pickering emulsion. *Int. J. Biol. Macromol.* **2022**, *222*, 438−447.
(53) Lu, Y.; Li, J.; Ge, L. L.; Xie, W. Y.; Wu, D. F. Pickering emulsion stabilized with fibrous nanocelluloses: Insight into fiber flexibility-emulsifying capacity relations. *Carbohydr. Polym.* **2021**, *255*, No. 117483.
(54) Kalashnikova, I.; Bizot, H.; Bertoncini, P.; Cathala, B.; Capron, I. Cellulosic nanorods of various aspect ratios for oil in water Pickering emulsions. *Soft Matter* **2013**, *9*, 952−959.
(55) Zhang, Z.; Cheng, M.; Gabriel, M. S.; Teixeira Neto, Â. A.; Da Silva Bernardes, J.; Berry, R.; Tam, K. C. Polymeric hollow microcapsules (PHM) via cellulose nanocrystal stabilized Pickering emulsion polymerization. *J. Colloid Interface Sci.* **2019**, *555*, 489−497.
(56) Tang, J.; Lee, M. F. X.; Zhang, W.; Zhao, B.; Berry, R. M.; Tam, K. C. Dual Responsive Pickering Emulsion Stabilized by Poly[2-(dimethylamino)ethyl methacrylate] Grafted Cellulose Nanocrystals. *Biomacromolecules* **2014**, *15*, 3052−3060.
(57) Liu, L.; Hu, Z.; Sui, X.; Guo, J.; Cranston, E. D.; Mao, Z. Effect of Counterion Choice on the Stability of Cellulose Nanocrystal Pickering Emulsions. *Ind. Eng. Chem. Res.* **2018**, *57*, 7169−7180.
(58) Foster, E. J.; Moon, R. J.; Agarwal, U. P.; Bortner, M. J.; Bras, J.; Camarero-Espinosa, S.; Chan, K. J.; Clift, M.; Cranston, E. D.; Eichhorn, S. J.; et al. Current characterization methods for cellulose nanomaterials. *Chem. Soc. Rev.* **2018**, *47*, 2609−2679.
(59) Kalashnikova, I.; Bizot, H.; Cathala, B.; Capron, I. New Pickering Emulsions Stabilized by Bacterial Cellulose Nanocrystals. *Langmuir* **2011**, *27*, 7471−7479.
(60) Mikulcová, V.; Bordes, R.; Minařík, A.; Kašpárková, V. Pickering oil-in-water emulsions stabilized by carboxylated cellulose nanocrystals − Effect of the pH. *Food Hydrocolloids* **2018**, *80*, 60−67.
(61) Kalashnikova, I.; Bizot, H.; Cathala, B.; Capron, I. Modulation of Cellulose Nanocrystals Amphiphilic Properties to Stabilize Oil/Water Interface. *Biomacromolecules* **2012**, *13*, 267−275.
(62) Cunha, A. G.; Mougel, J.-B.; Cathala, B.; Berglund, L. A.; Capron, I. Preparation of Double Pickering Emulsions Stabilized by Chemically Tailored Nanocelluloses. *Langmuir* **2014**, *30*, 9327−9335.
(63) Capron, I.; Rojas, O. J.; Bordes, R. Behavior of nanocelluloses at interfaces. *Curr. Opin. Colloid Interface Sci.* **2017**, *29*, 83−95.
(64) Guo, S.; Zhu, Y.; Xu, W.; Huan, S.; Li, J.; Song, T.; Bai, L.; Rojas, O. J. Heteroaggregation effects on Pickering stabilization using oppositely charged cellulose nanocrystal and nanochitin. *Carbohydr. Polym.* **2023**, *299*, No. 120154.
(65) Bai, L.; Lv, S.; Xiang, W.; Huan, S.; McClements, D. J.; Rojas, O. J. Oil-in-water Pickering emulsions via microfluidization with cellulose nanocrystals: 1. Formation and stability. *Food Hydrocolloids* **2019**, *96*, 699−708.
(66) Yuan, T.; Zeng, J.; Wang, B.; Cheng, Z.; Chen, K. Pickering emulsion stabilized by cellulosic fibers: Morphological properties-interfacial stabilization-rheological behavior relationships. *Carbohydr. Polym.* **2021**, *269*, No. 118339.
(67) Jiménez-Saelices, C.; Trongsatitkul, T.; Lourdin, D.; Capron, I. Chitin Pickering Emulsion for Oil Inclusion in Composite Films. *Carbohydr. Polym.* **2020**, *242*, No. 116366.
(68) Meirelles, A. A. D.; Costa, A. L. R.; Cunha, R. L. The stabilizing effect of cellulose crystals in O/W emulsions obtained by ultrasound process. *Food Res. Int.* **2020**, *128*, No. 108746.

https://doi.org/10.1021/acsomega.2c08239
ACS Omega 2023, 8, 15114−15123